Dalton Transactions

Accepted Manuscript

ROYAL SOCIETY OF CHEMISTRY

www.rsc.org/dalton

Graphical Abstract

Photocatalytic Activity of Transition-Metal-Ion-Doped Coordination Polymer (CP): Photoresponse Region Extension and Quantum Yields Enhancement via the Doping of Transition Metal Ion into the Framework of CPs

Xin-Xin Xu, Zhong-Ping Cui, Xin Gao and Xiao-Xia Liu*

Department of Chemistry, College of Science, Northeast University, Shenyang, Liaoning, 110819, People's Republic of China

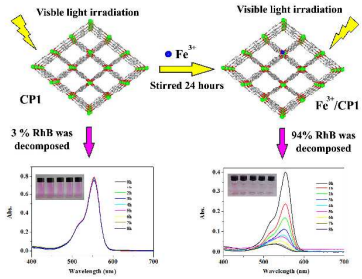

To enhance the photocatalytic activity of **CP1** and **TMI/CP1** were synthesized and their photocatalytic activities were studied.

Photocatalytic Activity of Transition-Metal-Ion-Doped Coordination Polymer (CP): Photoresponse Region Extension and Quantum Yields Enhancement via the Doping of Transition Metal Ion into the Framework of CPs

Xin-Xin Xu, Zhong-Ping Cui, Xin Gao and Xiao-Xia Liu*

Department of Chemistry, College of Science, Northeast University, Shenyang, Liaoning, 110819, People's Republic of China

*Author to whom correspondence should be addressed.

Tel: +86-024-83689510, Fax: +86-024-23600159.

E-mail: xxliu@mail.neu.edu.cn (Professor X. X. Liu).

Abstract

To improve photocatalytic activity of a coordination polymer (**CP**) in visible light region, five different transition metal ions (Fe^{3+}, Cr^{3+}, Ru^{3+}, Co^{2+} and Ni^{2+}) were introduced into its framework through an ion-exchange process. Among all the resulting transition metal ion doped coordination polymers (**TMI/CPs**), the one doped with Fe^{3+} took on the most excellent photocatalytic activity and highest quantum yields in visible light region, decomposing 94% Rhodamine B (RhB) in 8 hours. It can be attributed to the doping of Fe^{3+}, which reduced the band gap (E_g) of the original CP, facilitating photocatalysis of the obtained polymer. Compared with the coordination polymer with Fe^{3+} as a dopant, products doped with other metal ions presented weaker photocatalytic activities in visible light region; while under the irradiation of ultraviolet light, they showed favorable photocatalytic properties. The results suggest that to dope transition metal ions into the framework of **CPs** would be an ideal option to enhance the photocatalytic activity of coordination polymers.

Introduction

Increasing contamination of organic dyes has been urging researchers to develop more efficient methods for their treatment.[1, 2] In this aspect, photocatalysis has attracted considerable attention for its ambient operation condition and reduced economic cost for the decomposition of recalcitrant contaminants.[3] Up to now, a number of classical photocatalysts such as TiO_2 and ZnO have been thoroughly explored and broadly applied in the degradation of organic dyes.[4] In addition to these traditional photocatalysts, researchers are working on novel photocatalyst, which are expected to bear more excellent photocatalytic activity.[5] Recently, the photocatalytic property of **CPs** has been a focus of research concerning photocatalysis.[6] Compared with traditional photocatalysts, **CPs** are endowed with more satisfactory photocatalytic efficiency and stability,[7] making it a burgeoning candidate photocatalyst for the nontoxic decomposition of organic dyes.[8] Although **CPs** possesses such merits as high stability, its poor photoresponse in visible light region hinders its further exploration and application.[9] Now, how to boost the photocatalytic activity in visible light region has become a significant problem in the investigation of **CPs**.

To strengthen the photocatalytic activity of a photocatalyst in visible light region, a feasible approach is to dope some specific transition metal ions into its framework.[10] Compared with the photocatalyst undone, the doped ones possess narrower band gap (E_g), which may accelerate its photocatalytic activity in visible light region. As to this, transition metal ions, such as Fe^{3+}, Cu^{2+}, Cr^{3+}, Ru^{3+}, Co^{2+} and Ni^{2+} have been employed to improve the photocatalytic activity of TiO_2, achieving favorable results.[11] Inspired by this, we deduced that the doping of transition metal ions into the framework of **CPs** could also lead to a bathochromic shift of the photoresponse region,

and its photocatalytic activity might get enhanced in visible light region.

Our assumption was confirmed to be reasonable by the fabrication of a series of **TMI/CPs**, named **Fe^{3+}/CP1**, **Cr^{3+}/CP1**, **Ru^{3+}/CP1**, **Co^{2+}/CP1** and **Ni^{2+}/CP1,** respectively, which were synthesized through the replacement of Zn^{2+} with Fe^{3+}, Cr^{3+}, Ru^{3+}, Co^{2+} and Ni^{2+} in the framework of a new **CP**, $[Zn(cca)(4,4'\text{-bipy})]_n$ (**CP1**) (cca = 4-carboxycinnamic dianion, 4,4'-bipy = 4,4'-bipyridine). The photocatalytic activity of these transition metal ion doped products were investigated for the degradation of RhB and the results indicate that **Fe^{3+}/CP1** exhibited the most excellent photocatalytic properties in visible and ultraviolet light region. Compared with **Fe^{3+}/CP1**, the photocatalytic efficiency of Ru^{3+}-, Cr^{3+}-, Co^{2+}- and Ni^{2+}-doped products were lower in visible light region, but they still exhibited outstanding photocatalytic activity under the irradiation of ultraviolet light. Up to now, different metal ions have been doped into the framework of **CPs** to improve their physical and chemical properties, but this "doping strategy" has never been employed to improve the photocatalytic activity of **CPs**, so it is believed that the fabrication of **TMI/CP** for enhanced photocatalysis has set a precedent.[12-14]

Experimental

Materials and synthesis

All purchased chemicals were of reagent grade and used without further purification. Elemental analyses (C, H, and N) were performed on a Perkin-Elmer 2400 CHN elemental analyzer. ICP (Zn, Fe, Cr, Ru, Co and Ni) was measured by a Thermo Jarrell-Ash ICP-9000(N+M). PXRD patterns were recorded on a Siemens D5005 diffractometer with Cu KR (λ=1.5418 Å) radiation. XPS was performed on a VG ESCALAB-MKII spectrometer with Al Kr X-ray radiation as the X-ray source for excitation. Diffuse reflectance spectra (DRS) were recorded on a Shimadzu-2501PC

spectrometer using $BaSO_4$ as a standard. The UV-visible adsorption spectrum was recorded using a Hitachi U-3010 UV-visible spectrometer. Nitrogen adsorption/desorption isotherms were measured using a Micromeritics ASAP 2020M volumetric gas sorption instrument and 99.999% pure N_2. FTIR spectra were recorded in the range of 4000-400 cm^{-1} on an Alpha Centaur FTIR spectrophotometer using KBr pellets. TGA were carried out on a Perkin-Elmer TG-7 analyzer heated from room temperature to 800 ºC at a ramp rate of 10 °C/min under nitrogen.

Synthesis of $[Zn(cca)(4,4'\text{-bipy})]_n$ (CP1)

CP1 was prepared from the mixture of $Zn(NO_3)_2{\cdot}6H_2O$ (0.030 g, 0.1 mmol), H_2cca (0.019 g, 0.1 mmol), 4,4'-bipy (0.016 g, 0.1 mmol), and 5 mL H_2O. The pH value of the mixture was adjusted to 6 with 1M NaOH with constant stir. Then the pH-value-adjusted mixture was transferred to a 15 mL Teflon-lined stainless steel bomb and kept at 180˚C under autogenously atmospheric pressure for 4 days. The reaction system was cooled to room temperature in the course of the next 24 hours. A large amount of block yellow crystals of **CP1** were obtained. Yield: 81% (based on Zn). Anal. Calcd for $C_{15}H_{10}NO_4Zn$: C, 53.99%; H, 3.02%; N, 4.20%. Found: C, 53.87%; H, 3.10%; N, 4.25%.

Preparation of TMI/CPs

Transition metal ion doped coordination polymers were prepared through an ion-exchange reaction. In a typical synthesis process, 0.12 g **CP1** was dispersed in 15mL 0.01 M solution of $Fe(NO_3)_3{\cdot}6H_2O$, $Cr(NO_3)_3{\cdot}9H_2O$, $Ru(NO_3)_3{\cdot}4H_2O$, $Co(NO_3)_3{\cdot}6H_2O$ and $Ni(NO_3)_3{\cdot}6H_2O$, respectively; after being stirred for 24 h, the resulting powders were recovered by centrifugation, followed by being rinsed with water repeatedly, and then stayed at 60˚C for 12 h to get dried. The final samples were then labeled as **Fe^{3+}/CP1**, **Cr^{3+}/CP1**, **Ru^{3+}/CP1**, **Co^{2+}/CP1** and **Ni^{2+}/CP1**,

respectively. Anal. for **Fe^{3+}/CP1**: C, 54.05%; H, 3.02%; N, 4.20%; Zn, 19.03%; Fe, 0.50%; for **Cr^{3+}/CP1**: C, 54.10%; H, 3.03%; N, 4.21%; Zn, 18.75%; Cr, 0.70%; for **Ru^{3+}/CP1**: C, 53.86%; H, 3.01%; N, 4.19%; Zn, 19.06%; Ru, 0.76%; for **Co^{2+}/CP1**: C, 54.04%; H, 3.02%; N, 4.20%; Zn, 18.93%; Co, 0.62%; **Ni^{2+}/CP1**: C, 54.03%; H, 3.02%; N, 4.20%; Zn, 19.02%; Ni, 0.53%.

Photocatalytic activity study

The photocatalytic activities of the samples were evaluated by the degradation of RhB in the aqueous solution. The aqueous solution of 80 ml 10^{-5} M RhB was mixed with 20 mg photocatalysts. The suspension containing RhB and photocatalyst were magnetically stirred in a dark condition for 40 min till an adsorption-desorption equilibrium was established, followed by the mixture being exposed to illumination and meanwhile the reaction starting. Samples were taken out regularly from the reactor and centrifuged immediately for separation of any suspended solid since then. The transparent solution was analyzed by a UV-vis spectrometer. For the analysis, a 300 W medium pressure mercury lamp served as a ultraviolet light source and a 300 W medium pressure mercury lamp with a cutoff filter ($\lambda \geq 420$ nm) served as a visible-light source.

Electrochemical measurements

Photoelectrochemical tests were carried out with a conventional three-electrode system in quartz cell filled with 0.1 M Na_2SO_4 electrolyte (100 mL). The **CP1/ITO** or **TMID/CP1/ITO** electrode served as the working electrode. The counter and reference electrodes were a Pt plate and a saturated calomel electrode (SCE) respectively. A 300 W Xe lamp with a cutoff filter ($\lambda \geq 420$ nm) was used as the excitation light source for visible irradiation. For incident photonto-electron

conversion efficiency (IPCE) measurements, a solution of 0.05 M I_2 and 0.5 M LiI in propylene carbonate was used as an electrolyte. The monochromatic light was from a 300 W Xe lamp, which was passed through a grating monochromator and the wavelength was selected at 5 nm intervals between 280 and 600 nm.

X-ray crystallography

Suitable single crystals of **CP1** was carefully selected under an optical microscope and glued on glass fibers. Structural measurement was performed on a Bruker AXS SMART APEX II CCD diffractometer at 293 K. The structures were solved by the direct method and refined by the full-matrix least-squares method on F^2 using the SHELXTL 97 crystallographic software package.[15] Anisotropic thermal parameters were used to refine all non-hydrogen atoms. Carbon-bound hydrogen atoms were placed in geometrically calculated positions; oxygen-bound hydrogen atoms were located in the difference Fourier maps, kept in that position and refined with isotropic temperature factors. The X-ray structural analysis is given in Table 1. Selected bond lengths and angles are listed in Table 2. Further details of the crystal structure determination have been deposited to the Cambridge Crystallographic Data Centre.

Results and discussion

Structure characterization and study

Single crystal X-ray analysis reveals that **CP1** adopts a 3-fold interpenetrated *a*-Po structure. There exists only one crystallographically independent Zn atom in the fundamental unit which is coordinated by four carboxylic oxygen atoms of cca ligands (Zn-O bond distances range from 2.028(3) to 2.076(3) Å) and one nitrogen atom of 4,4'-bipy ligand (Zn-N bond distance is 2.053(4) Å). This furnishes a square-pyramidal geometry of Zn1. Two crystallographically equivalent Zn atoms are bridged by four carboxylates and give a paddle-wheel shaped $[Zn_2(CO_2)_4]$ fragment

with a Zn···Zn distance of 2.982(11) Å. The axis sites of each Zn_2 paddle wheel are occupied by two nitrogen atoms from 4,4'-bipy ligands. Such arrangement of the carboxylates and nitrogen atoms results in an octahedral $[Zn_2(CO_2)_4N_2]$ SBU. Each octahedral SBU is connected to six others through four bridging cca and two 4,4'-bipy to generate an extended neutral 3D *α*-Po network. Owing to the great lengths of cca and 4,4'-bipy ligands, there exists large cube-like cavity with dimensions of approximately 13.2 Å × 13.2 Å × 11.2 Å in the framework (Fig. 1b). These large voids allow incorporation of the other two identical networks, which leads to a 3-fold interpenetrated *α*-Po network (Fig. 1c). To our knowledge, among currently known interpenetrated coordination polymers with *α*-Po topology, the majority are of 2-fold, and only a few 3-fold interpenetrated examples have been reported until now.[16, 17] Although interpenetration has blocked the channels along the *a* and *b* axis, a channel with a cavity window size of about 7.8 Å × 8.4 Å still remains along the *c* axis (Fig. 1d). The permanent porosity of **CP1** was demonstrated by N_2 sorption studies, the BET and Langmuir surface areas are 206 and 243 m^2/g, respectively (Fig. S1, ESI). This makes **CP1** a suitable host for the doping of transition metal ions such as Fe^{3+}, Cr^{3+}, Ru^{3+}, Co^{2+} and Ni^{2+}.[18] Furthermore, **CP1** exhibited great thermal stability, keeping stable at about 350 ˚C (Fig. S2).

The structures of **Fe^{3+}/CP1**, **Cr^{3+}/CP1**, **Ru^{3+}/CP1**, **Co^{2+}/CP1** and **Ni^{2+}/CP1** were studied with PXRD, which took on approximately similar diffraction patterns to **CP1** merely with some peaks weakened. This implies that although the substitution of Zn^{2+} by transition metal ions decreased the crystallization of **CP1**, its structure was still well retained and its crystalline nature was not destroyed (Fig. 2a). Such conclusion can also be drawn from IR spectra, which kept unchanged before and after doping (Fig. S3). It is also noticed that compared with pure **CP1**, the peaks of **Fe^{3+}/CP1** and

Cr^{3+}/CP1 both shifted to higher degree region. This confirms that Fe^{3+} and Cr^{3+} were doped into the crystal lattice of **CP1**, because the ionic radius of Fe^{3+} (0.64 Å) and Cr^{3+} (0.63 Å) are remarkably smaller than Zn^{2+} (0.74 Å). Consequently, the unit cell would shrink distinctly, and shifts to higher angle region would occur when Fe^{3+} and Cr^{3+} were doped into the framework of **CP1** (Fig. 2b).[19] For **Ru^{3+}/CP1**, **Co^{2+}/CP1** and **Ni^{2+}/CP1**, the positions of their diffraction peaks were almost not changed before and after doping, which could be ascribed to the similar ionic radius of Ru^{3+} (0.71 Å), Co^{2+} (0.73 Å) and Ni^{2+} (0.70 Å) to Zn^{2+}.

The XPS spectra of **CP1** and its transition metal doped products were studied to examine the valence state as well as existing form of these dopants (Fig. 3). For **CP1**, the Zn $2p_{3/2}$ and Zn $2p_{1/2}$ peaks were located at 1022.3 and 1045.4 eV, respectively. But after the doping of transition metal ions into the framework of **CP1**, these peaks shifted to higher energies. For **Fe^{3+}/CP1**, **Cr^{3+}/CP1**, **Ru^{3+}/CP1**, **Co^{2+}/CP1** and **Ni^{2+}/CP1**, Zn $2p_{3/2}$ and Zn $2p_{1/2}$ peaks appeared at 1024.8, 1047.8 eV; 1025.1, 1048.6 eV; 1025.2, 1048.4 eV; 1024.2, 1047.7 eV and 1024.1, 1047.6 eV, respectively. These movements could be attributed to the formation of new M^{n+}-O (M^{n+} = Fe^{3+}, Cr^{3+}, Ru^{3+}, Co^{2+} and Ni^{2+}) bonds in the crystal lattice (Fig. 4).[20a] In addition to the above peaks belonging to Zn^{2+}, the peaks appeared at 711.6, 725.1 eV; 577.4, 587.2 eV; 289.4 eV; 780.3, 795.1 eV and 856.5, 872.8 eV could be attributed to Fe $2p_{3/2}$, Fe $2p_{1/2}$; Cr $2p_{3/2}$, Cr $2p_{1/2}$; Ru $3d_{3/2}$; Co $2p_{3/2}$, Co $2p_{1/2}$ and Ni $2p_{3/2}$, Ni $2p_{1/2}$, respectively (Fig. 3, inset). But compared with pure Fe^{3+}, Cr^{3+}, Ru^{3+}, Co^{2+} and Ni^{2+}, in **Fe^{3+}/CP1**, **Cr^{3+}/CP1**, **Ru^{3+}/CP1**, **Co^{2+}/CP1** and **Ni^{2+}/CP1**, binding energies of these elements also shifted to higher energy levels. These results indicate that the transition metal ions were doped into **CP1**, substituting Zn^{2+} in the framework, and M^{n+}-O bonds formed.[20b]

Optical property

Diffuse reflectance spectra (DRS) of **CPs**, **Fe^{3+}/CP1**, **Cr^{3+}/CP1**, **Ru^{3+}/CP1**, **Co^{2+}/CP1** and **Ni^{2+}/CP1** were studied. It was obvious that **CP1** merely took photoresponse in ultraviolet light region. After the doping of transition metal ions into the framework of **CP1**, Fe^{3+} and Ru^{3+} doped products showed enhanced photoresponse in visible light region, while the photoresponse of **Cr^{3+}/CP1**, **Co^{2+}/CP1** and **Ni^{2+}/CP1** was still in the ultraviolet light region (Fig. 5a).[21, 22] To study the photoresponse in detail, band gaps (E_g) of **CP1** and its transition metal ion doped products were calculated by Tauc equation. For **CP1**, its band gap is 3.14 eV (Fig. 6a), while band gaps of **Fe^{3+}/CP1**, **Cr^{3+}/CP1**, **Ru^{3+}/CP1**, **Co^{2+}/CP1** and **Ni^{2+}/CP1** are 2.72, 2.97, 2.88, 3.23 and 3.16eV, respectively (Fig 5b). For the **TMI/CPs**, the discrepancy in their band gaps should be attributed to the differences in energy level of the dopants. Among these five doped products, **Fe^{3+}/CP1** possessed the narrowest band gap, which illustrates that the doping of Fe^{3+} into the framework of **CP1** may be a feasible approach to enhance its photocatalytic behavior for solar energy application.

Electrochemical analysis

The interface charge separation efficiency was investigated by photocurrent spectra and incident photon-to-electron conversion efficiency (IPCE). Photocurrent responses of **CP1/ITO** and **TMI/CP1/ITO** electrodes were studied under ultraviolet and visible light irradiation (Fig. 6a). Results illustrate under irradiation of ultraviolet light, all these five **TMI/CP1/ITO** electrodes exhibit stronger photocurrent than **CP1/ITO** electrode. While under the irradiation of visible light, only **Fe^{3+}/CP1** and **Ru^{3+}/CP1** show enhanced photocurrent. In all these five **TMI/CP1** electrodes, **Fe^{3+}/CP1** electrode has the largest photocurrent.

TMI/CP1/ITO electrodes also exhibit remarkably improved IPCE than **CP1/ITO**

electrode (Fig. 6b). The maximum IPCE value (3.55%) of **CP1/ITO** electrode appeared at 365 nm. After the doping of Ru^{3+}, Cr^{3+}, Ni^{2+} and Co^{2+}, peaks of the resulting products kept unchanged, but their IPCE values enhanced greatly (7.27%, 6.57%, 4.96% and 4.74% for **Ru^{3+}/CP1**, **Cr^{3+}/CP1**, **Ni^{2+}/CP1** and **Co^{2+}/CP1** electrodes respectively). For **Fe^{3+}/CP1** electrode, its maximum IPCE (13.17%) shifted to 425 nm. These results illustrate the doping of transition metal ions into the framework of **CP1** leads to an effective charge separation and transfer process in the resulting products. Either in ultraviolet or visible light region, **Fe^{3+}/CP1** possesses the highest photogenerated charge separation efficiency.

Photocatalytic property study

The photocatalytic activities of **CP1** and its metal ion doped products were evaluated by the degradation of RhB in aqueous solution (Fig. 7a and 7b). When **CP1** acted as the catalyst, under the irradiation of ultraviolet light, about 34% RhB decomposed in 8 h; while in visible light region, RhB could not be degraded by **CP1**. As for polymers with transition metal ions as dopants, their photocatalytic activities were improved markedly. Among them all, **Fe^{3+}/CP1** displayed the first-rate photocatalytic properties, decomposing 88% and 94% RhB in 8 h under the irradiation of ultraviolet and visible light, respectively. **Ru^{3+}/CP1** also bore photocatalytic activity in visible light region, degrading 21% RhB in 8 h. In the ultraviolet light region, the photocatalytic efficiency of **Ru^{3+}/CP1** was much higher than the others with about 75% RhB resolved for the same period. As for **Cr^{3+}/CP1**, **Co^{2+}/CP1** and **Ni^{2+}/CP1**, they could not decompose RhB in the visible light region, but in the ultraviolet light region, their photocatalytic properties were more standout than **CP1**, decomposing 63%, 68% and 76% RhB in 8 h, respectively. These results imply that

the introduction of different metal ions have diverse influences on the improvement of photocatalytic properties, and among these dopants, Fe^{3+} is the most ideal candidate to enhance the photocatalytic activity of **CP1**.

In photocatalytic degradation reaction, the activity of recycled catalyst is a very important factor to determine the performance of a photocatalyst. Here, the photocatalytic reaction of **Fe^{3+}/CP1** was re-examined five times under ultraviolet and visible light irradiation, and the recycled **Fe^{3+}/CP1** still showed satisfactory catalytic property (Fig. 7c and 7d). Furthermore, the recycled samples also exhibit similar PXRD patterns with original composite materials, which indicate their structures were not destroyed during the photocatalysis decomposition process of RhB (Figure 7e and 7f).This indicates its high stability during the RhB decomposition process.

Mechanism study

According to optical properties and photocatalytic performances of **CP1** and **TMI/CP1**, we can speculate their mechanism. For **CP1**, under the irradiation of ultraviolet light, electrons can be excited from the valence band (VB), transferring to the conduction band (CB), and simultaneously, positive charged holes are formed in valence band (Scheme 1a). After migrating to the surface of **CP1**, the electrons and holes can produce radical specials, such as super oxide radial and hydroxyl radicals, which are responsible for the degradation of RhB. After the doping of Fe^{3+} into the framework of **CP1**, a new energy level is formed between the CB of **CP1** and 3d orbital of Fe^{3+}, which can be considered as the CB of **Fe^{3+}/CP1** (Scheme 1b). For **Fe^{3+}/CP1**, its CB energy level is lower than **CP1**, but its VB energy level is retained and equal to **CP1**, leading to the reduction of band gap. So, for **Fe^{3+}/CP1**, it is possible to excite electrons from VB to the newly formed CB with lower energy than

that **CP1** needed. It can be concluded that the visible light activity of **Fe^{3+}/CP1** can be ascribed to the matching of the CB of **CP1** for the 3d orbital of Fe^{3+}. For **Cr^{3+}/CP1**, **Ru^{3+}/CP1**, **Co^{2+}/CP1** and **Ni^{2+}/CP1**, the weak photocatalytic activities under visible light may arise from mismatching of their 3d energy levels for the CB of **CP1** (Scheme 1c).[25]

Conclusions

With a simple ion-exchange process, Fe^{3+}, Cr^{3+}, Ru^{3+}, Co^{2+} and Ni^{2+} were doped into the framework of coordination polymer, respectively, and five transition-metal-ion-doped coordination polymers, **Fe^{3+}/CP1**, **Cr^{3+}/CP1**, **Ru^{3+}/CP1**, **Co^{2+}/CP1** and **Ni^{2+}/CP1** were prepared successfully. These **TMI/CPs** exhibited the same structural features even with different dopant ion resides in their frameworks. Although the introduction of transition metal ions can improve photocatalytic activities of coordination polymers, the structural diversity of these dopants has great influences on the photocatalytic performance of the resulting doped coordination polymers. It can be concluded that the doping of transition metal ions into the framework of coordination polymers enable us to establish a feasible approach to polishing up their photocatalytic properties and these doped coordination polymers are new efficient photocatalysts for the decontaminating and reusing of colored wastewater industrially produced.

Acknowledgements

We gratefully acknowledge financial supports from National Natural Science Foundation of China (21303010; 21273029); Research Foundation for the Doctoral Program of Higher Education of China (20120042110024) and Fundamental Research Funds for the Central Universities (N120405005).

Electronic supplementary information (ESI) available: N_2 gas-sorption curve of

CP1 at 77 K; TGA of **CP1**; IR of **CP1**, **Fe^{3+}/CP1**, **Cr^{3+}/CP1**, **Ru^{3+}/CP1**, **Co^{2+}/CP1** and **Ni^{2+}/CP1**; XPS spectrum of C, N and O elements in **CP1**, **Fe^{3+}/CP1**, **Cr^{3+}/CP1**, **Ru^{3+}/CP1**, **Co^{2+}/CP1** and **Ni^{2+}/CP1**; Absorption spectra of RhB degraded with **CP1**, **Fe^{3+}/CP1**, **Cr^{3+}/CP1**, **Ru^{3+}/CP1**, **Co^{2+}/CP1** and **Ni^{2+}/CP1** under irradiation of ultraviolet and visible light. Absorption spectra of RhB degraded with $Fe(NO_3)_3 \cdot 6H_2O$ under irradiation of visible light. CCDC reference numbers 899342 (**CP1**).

References

(1) (a) R. Asahi, T. Morikawa, T. Ohwaki, K. Aoki, Y. Taga, *Science* 2001, **293**, 269; (b) W. Zhao, W. H. Ma, C. C. Chen, J. C. Zhao, Z. G. Shuai, *J. Am. Chem. Soc*., 2004, **126**, 4782; (c) Y. Cong, J. L. Zhang, F. Chen, M. Anpo, *J. Phys. Chem. C*, 2007, **111**, 6976.

(2) (a) S. Kohtani, M. Koshiko, A. Kudo, K. Tokumura, Y. Ishigaki, A. Toriba, K. Hayakawa, R. Nakagaki, *Appl. Catal., B*, 2003, **46**, 573; (b) S. Kohtani, M. Tomohiro, K. Tokumura, R. Nakagaki, *Appl. Catal., B*, 2005, **58**, 265.

(3) (a) M. R. Hoffmann, S. T. Martin, W. Y. Choi, D. W. Bahnermann, *Chem. Rev*., 1995, **95**, 69; (b) A. L. Linsebigler; G. Q. Lu, J. T. Yates, *Chem. Rev*., 1995, **95**, 735; (c) T. Hiroaki, F. Musashi, K. Hisayoshi, *Chem. Soc. Rev*., 2011, **40**, 4230; (d) A. Hiskia, A. Mylonas, E. Papaconstantinou, *Chem. Soc. Rev*., 2001, **30**, 62; (e) D. Ravelli, D. Dondi, M. Fagnoni, A. Albini, *Chem. Soc. Rev*., 2009, **38**, 1999.

(4) (a) J. N. Schrauben, R. Hayoun, C. N. Valdez, M. Braten, L. Fridley, J. M. Mayer, *Science* 2012, **336**, 1298; (b) D. Lehr, M. Luka, M. R. Wagner, M. Buelger, A. Hoffmann, S. Polarz, *Chem. Mater*., 2012, **44**, 1771; (c) X. Zhang, C. L. Shao, Z. Y. Zhang, J. H. Li, P. Zhang, M. Y. Zhang, J. B. Mu, Z. C. Guo, P. P. Liang, Y. C. Liu, *Appl. Mater. Surf*., 2012, **4**, 785; (d) J. Manna, R. K. Rana, *Chem. Eur. J*., 2012, **18**, 498.

(5) (a) C. H. Kim, B. H. Kim, K. S. Yang, *Carbon* 2012, **50**, 2472; (b) Z. Yang, S. Y. Gao, H. F. Li, R. Cao, *J. Colloid Interface Sci*., 2012, **375**, 172; (c) A. A. Ismail, *Appl. Catal*., *B*, 2012, **117**, 67; (d) S. Civis, M. Ferus, M. Zukalova, P. Kubat, L. Kavan, *J. Phys. Chem. C*, 2012, **116**, 11200.

(6) (a) M. C. Das, H. Xu, Z. Y. Wang, G. Srinivas, W. Zhou, Y. F. Yue, V. N. Nesterov, G. D. Qian, B. L. Chen, *Chem. Commun*., 2011, **47**, 11715; (b) C. Wang, Z. G. Xie,

K. E. DeKrafft, W. B. Lin, *J. Am. Chem. Soc*., 2011, **133**, 13445; (c) C. G. Silva, I. Luz, F. X. L. Xamena, A. Corma, H. García, *Chem. Eur. J*., 2010, **16**, 11133; (d) C. G. Silva, A. Corma, H. García, *J. Mater. Chem*., 2010, **20**, 3141.

(7) P. Mahata, C. Madras, S. Natarajan, *J. Phys. Chem. C*, 2006, **110**, 13759.

(8) (a) K. X. Wang, J. S. Chen, *Acc. Chem. Res*., 2011, **44**, 531; (b) Z. T. Yu, Z. L. Liao, Y. S. Jiang, G. H. Li, J. S. Chen, *Chem. Eur. J*., 2005, **11**, 2642; (c) Z. T. Yu, Z. L. Liao, Y. S. Jiang, G. H. Li, G. D. Li, J. S. Chen, *Chem. Commun*., 2004, 1814; (d) Y. Xia, K. X. Wang, J. S. Chen, *Inorg. Chem. Commun*., 2010, **13**, 1542.

(9) (a) D. E. Wang, K. J. Deng, K. L. Lv, C. G. Wang, L. L. Wen, D. F. Li, *CrystEngComm*., 2009, **11**, 1442; (b) F. Wang, X. H. Ke, J. B. Zhao, K. J. Deng, X. K. Leng, Z. F. Rian, L. L. Wen, D. F. Li, *Dalton Trans*., 2011, **40**, 11856; (c) L. L. Wen, F. Wang, J. Feng, K. L. Lv, C. G. Wang, D. F. Li, *Cryst. Growth Des*., 2009, **9**, 3581; (d) H. Qu, L. Qiu, X. K. Leng, M. M. Wang, S. M. Lan, L. L. Wen, D. F. Li, *Inorg. Chem. Commun*., 2011, **14**, 1347.

(10) (a) M. I. Litter, *Appl. Catal., B*, 1999, **23**, 89; (b) J. C. Yu, G. S. Li, X. C. Wang, X. L. Hu, C. W. Leung, Z. D. Zhang, *Chem. Commun*., 2006, 2717.

(11) (a) H. Khajavi, J. Gascon, J. M. Schins, L. D. A. Aiebbeles, F. Kapteijn, *J. Phys. Chem. C*, 2011, **115**, 12487; (b) T. Tachikawa, J. R. Choi, M. Fujitsuka, T. Majima, *J. Phys. Chem. C*, 2008, **112**, 14090.

(12) (a) D. W. Rao, R. F. Lu, C. Y. Xiao, E. J. Kan, K. M. Deng, *Chem. Commun*., 2011, **47**, 7698; (b) D. Wu, Q. Xu, D. H. Liu, C. L. Zhong, *J. Phys. Chem. C*, 2010, **114**, 16611; (c) T. Stergiannakos, E. Tylianakis, E. Klontzas, P. Trikalitis, G. Froudakis, *J. Phys. Chem. C*, 2012, **116**, 8359.

(13) (a) W. Dai, J. Hu, L. M. Zhou, S. Li, X. Hu, H. Huang, *Source: Energy Fuels*, 2013, **27**, 816; (b) A. Ghoufi, J. Deschamps, G. Maurin, *J. Phys. Chem. C*,

2012, **116**, 10504; (c) C. Wang, Z. G. Xie, K. E. deKrafft, W. L. Lin, *J. Am. Chem. Soc*., 2011, **133**, 13445.

(14) (a) G. Zhang, F. F. Luo, X. F. Liu, G. P. Dong, Q. Zhang, G. Lin, Q. L. Zhou, J. R. Qiu, L. L. Hu, D. P. Chen, *Laser Phys*., 2010, **20**, 1425; (b) A. D. Guzman-Chavez, A. Diez, J.L. Cruz, M.V. Andres, *Laser Phys*., 2012, **22**, 579; (c) Y. X. Zhou, X. Y. Yu, X. C. Xu, S. X. Dai, *Acta Phys. Sinica*., 2012, **61**, 157701.

(15) (a) G. M. Sheldrick, SHLEXL97, *Program for Crystal Structure Refinement*, University of Göttingen, Germany, 1997; (b) G. M. Sheldrick, SHLEXL97, *Program for Crystal structure Solution*, University of Göttingen, Germany, 1997.

(16) (a) T. Soma, H. Yuge, T. Iwamoto, *Angew. Chem*., 1994, **106**, 1746; *Angew. Chem. Int. Ed*., 1994, **33**, 1665; (b) M. J. Plater, M. R. S. J. Foreman, J. M. S. Skakle, *Cryst. Eng*., 2001, **4**, 293.

(17) (a) B. F. Abrahams, B. F. Hoskins, R. Robson, D. A. Slizys, *CrystEngComm*., 2002, **4**, 478; (b) X. L. Wang, C. Qin, E. B. Wang, Z. M. Su, *Chem. Eur. J*., 2006, **12**, 2680.

(18) (a) L. Chen, K. Tan, Y. Q. Lan, S. L. Li, K. Z. Shao, Z. M. Su, *Chem. Commun*., 2012, **48**, 5919; (b) J. H. Cui, Z. Z. Lu, Y. Z. Li, Z. J. Guo, H. G. Zheng, *Chem. Commun*., 2012, **48**, 7967; (c) Z. Y. Guo, H. Xu, S. Q. Su, J. F. Cai, S. Dang, S. C. Xiang, G. D. Qian, H. J. Zhang, M. O'Keeffe, B. L. Chen, *Chem. Commun*., 2011, **47**, 5551; (d) Y. Q. Xiao, Y. J. Cui, Q. Zheng, S. C. Xiang, G. D. Qian, B. L. Chen, *Chem. Commun*., 2010, **46**, 5503.

(19) (a) K. Nagaveni, M. S. Hegde, G. Madras, *J. Phys. Chem. B*., 2004, **108**, 20204; (b) X. M. Sun, Y. D. Li, *Chem. Eur. J*., 2003, **9**, 2229.

(20) (a) D. F. Wang, J. H. Ye, T. Kako, T. Kimura, *J. Phys. Chem. B*., 2006, **110**, 15824; (b) J. F, Zhu, Z. G. Deng, F. Chen, J. L. Zhang, H. J. Chen, M. Anpo, J. Z.

Huang, L.Z. Zhang, *Appl. Catal., B*, 2006, **62**, 329.

(21) (a) R. Konta, T. Ishii, H. Kato, A. Kudo, *J. Phys. Chem. B*, 2004, **108**, 8992; (b) W. Y. Choi, A. Termin, M. R. Hoffmann, *J. Phys. Chem*, 1994, **98**, 13669; (c) M. Yang, X. L. Huang, S. C. Yan, Z. S. Li, T. Yu, Z. G. Zou, *Mater. Chem. Phys*., 2010, **121**, 506.

(22) (a) T. H. Xie, X. Y. Sun, J. Lin, *J. Phys. Chem. C*, 2008, **112**, 14090; (b) A. Fuerte, M. D. Hernández-Alonso, A. J. Maira, A. Martínez-Arias, M. Fernández-García, J. C. Conesa , J. Soria, *Chem. Commun*., 2001, 2718.

(23) (a) B. Wu, Z. G. Ren, H. X. Li, M. Dai, D. X. Li, Y. Zhang, J. P. Lang, *Inorg. Chem. Commun*., 2009, **12**, 1168; (b) Z. Su, J. Fan, M. Chen, T. Okamura, W. Y. Sun, *Cryst. Growth Des*., 2011, **11**, 1159.

(24) (a) L. Song, R. L. Qiu, Y. Q. Mo, D. D. Zhang, H. Wei, Y. Xiong, *Catal Commun*., 2007, **8**, 429; (b) T. J. Savenije, J. M. Warman, A. Goossens, *Chem. Phys. Lett*., 1998, **287**, 148; (c) J. S. Salafsky, W. H. Lubberhuizen, R. E. I. Schropp, *Chem. Phys. Lett*., 1998, **290**, 297; (d) A. C. Arango, S. A. Carter, P. J. Brock, *Appl. Phys. Lett*., 1999, **74**, 1698.

(25) A. D. Paola, E. García-López, S. Ikedab, G. Marcì, B. Ohtani, L. Palmisano, *Catal. Today* 2002, **75**, 87.

Table 1 Crystal data and structure refinement results for **CP1**

Empirical formula	$C_{15}H_{10}NO_4Zn$
Formula weight	333.61
Crystal system	Monoclinic
Space group	*C* 2/c
a/Å	16.752(5)
b/Å	20.392(6)
c/Å	10.355(3)
β/º	115.486(4)
V/Å^3	3193.2(16)
Z	8
D_{calcd}/(g cm^{-3})	1.388
F (000)	1352
Reflections collected	9781
Reflections unique	2771
R (int)	0.0211
Goodness-of-fit on F^2	1.059
R_1 [$I > 2\sigma(I)$]	0.0506
wR_2 [$I > 2\sigma(I)$]	0.1658
R_1 (all data)	0.0557
wR_2 (all data)	0.1744

Note. $R_1 = \Sigma||F_o|-|F_c||/\Sigma|F_o|$; $wR_2 = \Sigma[w(F_o^2-F_c^2)^2]/\Sigma[w(F_o^2)^2]^{1/2}$

Table 2 Selected bond lengths (Å) and angles (º) for **CP1**

Zn(1)-O(1)#3	2.076(3)	Zn(1)-O(2)	2.036(3)
Zn(1)-O(3)#1	2.028(3)	Zn(1)-O(4)#2	2.048(3)
Zn(1)-N(1)	2.053(4)		
O(2)-Zn(1)-O(1)#3	86.01(13)	O(2)-Zn(1)-O(4)#2	90.11(15)
O(2)-Zn(1)-N(1)	97.86(12)	O(3)#1-Zn(1)-O(1)#3	88.05(15)
O(3)#1-Zn(1)-O(2)	165.49(13)	O(3)#1-Zn(1)-O(4)#2	89.02(15)
O(4)#2-Zn(1)-O(1)#3	152.36(13)	O(3)#1-Zn(1)-N(1)	96.58(13)
O(4)#2-Zn(1)-N(1)	98.95(13)	N(1)-Zn(1)-O(1)#3	108.69(13)

Symmetry transformations used to generate equivalent atoms for **CP1**: #1: x-1/2, y-1/2, z; #2: -x+3/2, y-1/2, -z+5/2; #3: -x+1, y, -z+5/2

Table 3 Values of degradation efficiency (η) of RhB with **CP1** and **TMI/CP1**

Catalyst	Time (hour)	Condition	η	Condition	η
CP1	8	ultraviolet light	33%	visible light	3%
Fe^{3+}/CP1	8	ultraviolet light	88%	visible light	94%
Cr^{3+}/CP1	8	ultraviolet light	75%	visible light	5%
Ru^{3+}/CP1	8	ultraviolet light	75%	visible light	20%
Co^{2+}/CP1	8	ultraviolet light	67%	visible light	3%
Ni^{2+}/CP1	8	ultraviolet light	63%	visible light	3%

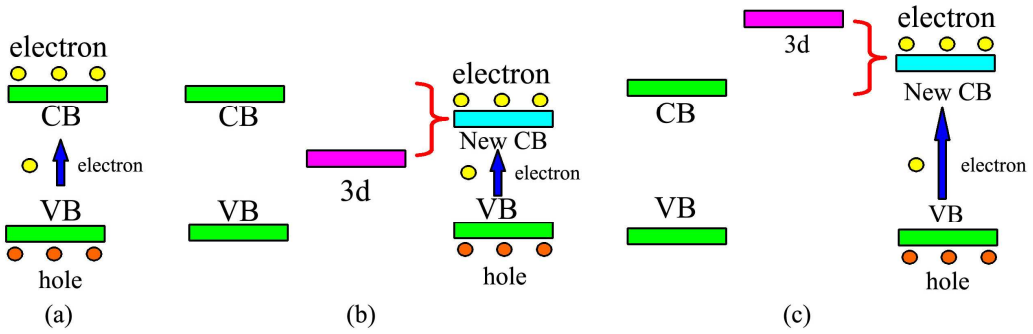

Scheme 1

Diagram of the photocatalytic mechanism: (a) **CP1** under ultraviolet light irradiation; (b) **Fe^{3+}/CP1** and **Ru^{3+}/CP1** under visible light irradiation; (c) **Cr^{3+}/CP1**, **Co^{2+}/CP1** and **Ni^{2+}/CP1** under visible light irradiation.

Figure Captions

Figure 1 (a) The fundamental unit of **CP1**; (b) 3D framework of **CP1**; (c) 3-fold interpenetration network of **CP1**; (d) 3D porous framework of **CP1**.

Figure 2 (a) PXRD of **CP1** and doped **CP1**; (b) PXRD of **CP1** and doped **CP1** in (0, 2, 0) and (1, 1, -1) direction.

Figure 3 XPS spectrum of doped **CP1** and **CP1** (survey): (a) **Fe^{3+}/CP1**, (b) **Cr^{3+}/CP1**, (c) **Ru^{3+}/CP1**, (d) **Co^{2+}/CP1**, (e) **Ni^{2+}/CP1** and (f) **CP1**; (inset, doped elements in **Fe^{3+}/CP1**, **Cr^{3+}/CP1**, **Ru^{3+}/CP1**, **Co^{2+}/CP1** and **Ni^{2+}/CP1** respectively).

Figure 4 XPS spectrum of Zn elements in doped **CP1** and **CP1**: (a) **Fe^{3+}/CP1**, (b) **Cr^{3+}/CP1**, (c) **Ru^{3+}/CP1**, (d) **Co^{2+}/CP1**, (e) **Ni^{2+}/CP1** and (f) **CP1**.

Figure 5 DRS of (a) **CP1** and **TMI/CP1**; (b) Eg of **CP1** and **TMI/CP1**.

Figure 6 (a) Photocurrent spectra of **CP1/ITO** and **TMI/CP1/ITO** under ultraviolet light; (a) Photocurrent spectra of **CP1/ITO** and **TMI/CP1/ITO** under ultraviolet light; (c) IPCE of **CP1/ITO** and **TMI/CP1/ITO** electrodes.

Figure 7 (a) Degradation rate for RhB as the function of irradiation time by **CP1** and **TMI/CP1** under ultraviolet light; (b) Degradation rate for RhB as the function of irradiation time by **CP1** and **TMI/CP1** under visible light; (c) Cycling runs of the degradation of RhB in the presence of **Fe^{3+}/CP1** under ultraviolet light; (d) Cycling runs of the degradation of RhB in the presence of **Fe^{3+}/CP1** visible light; (d) PXRD of recycled **Fe^{3+}/CP1** under ultraviolet light; (d) PXRD of recycled **Fe^{3+}/CP1** under visible light.

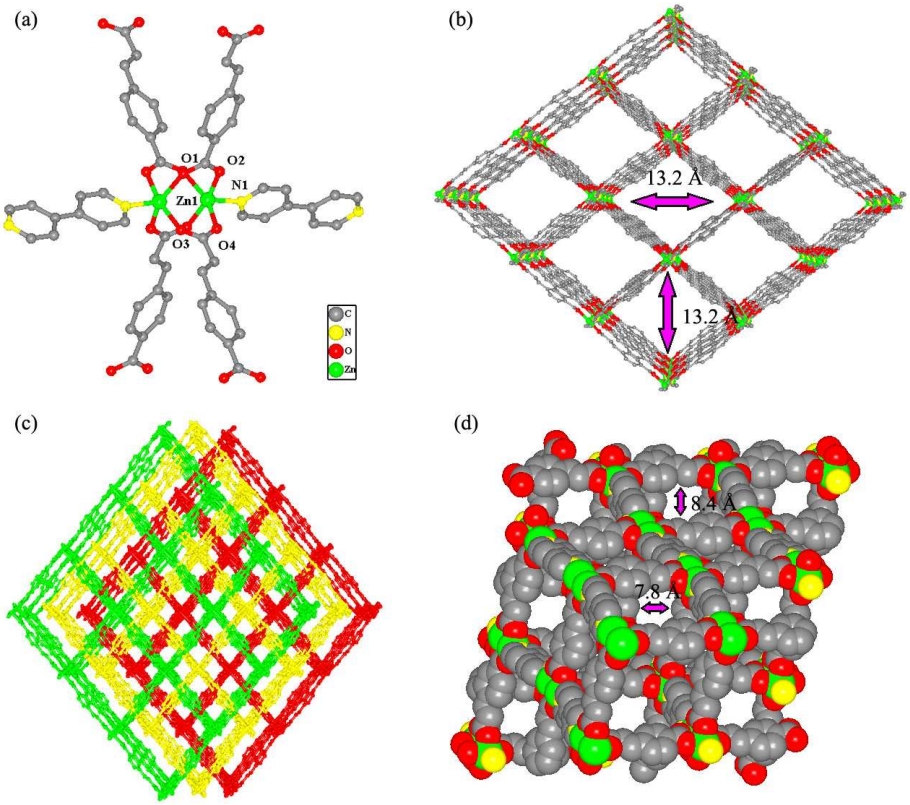

Figure 1

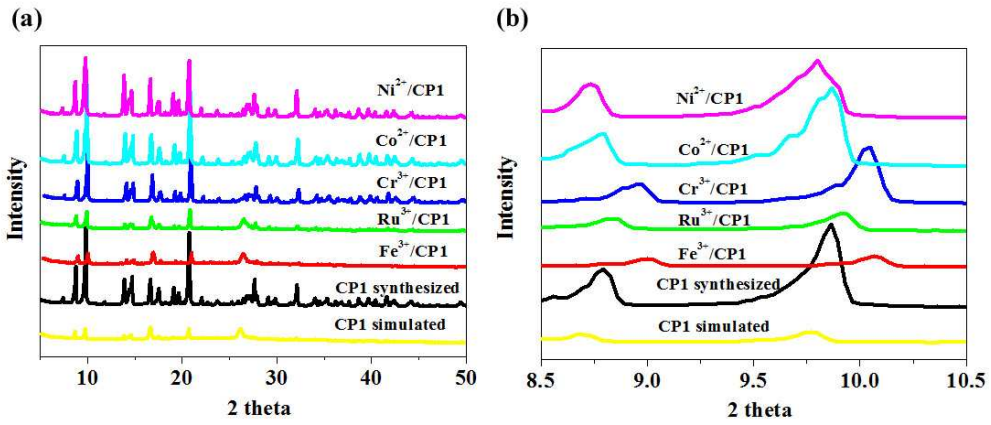

Figure 2

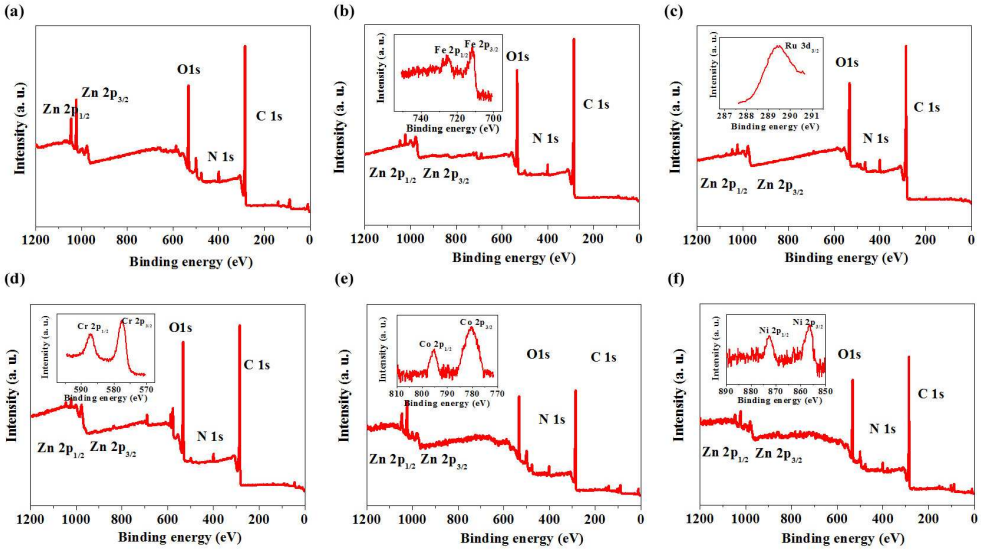

Figure 3

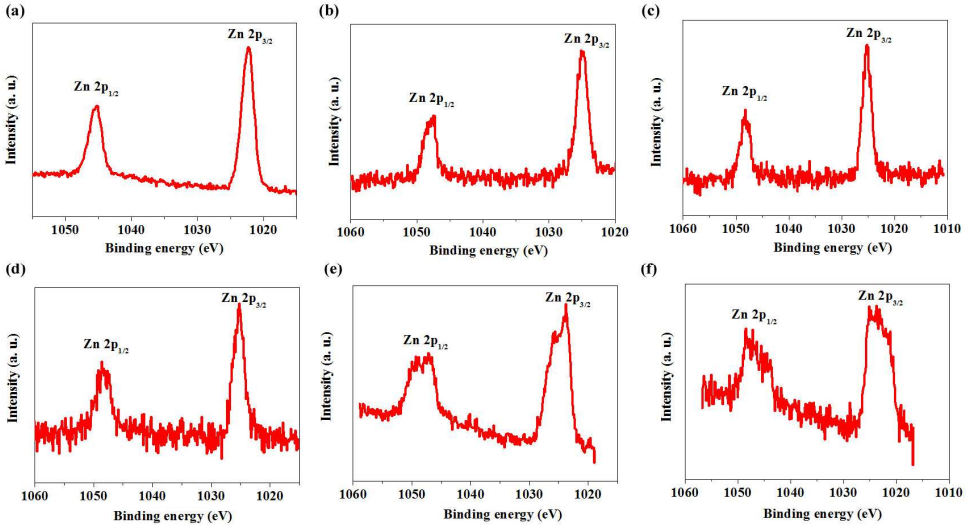

Figure 4

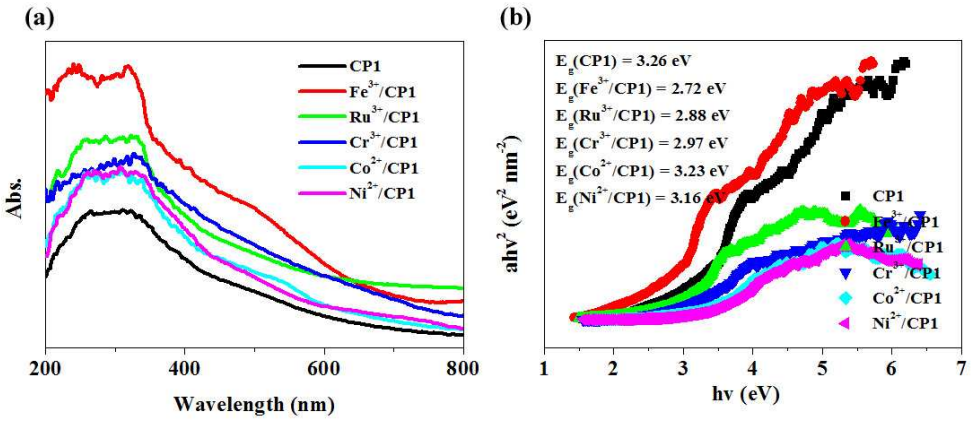

Figure 5

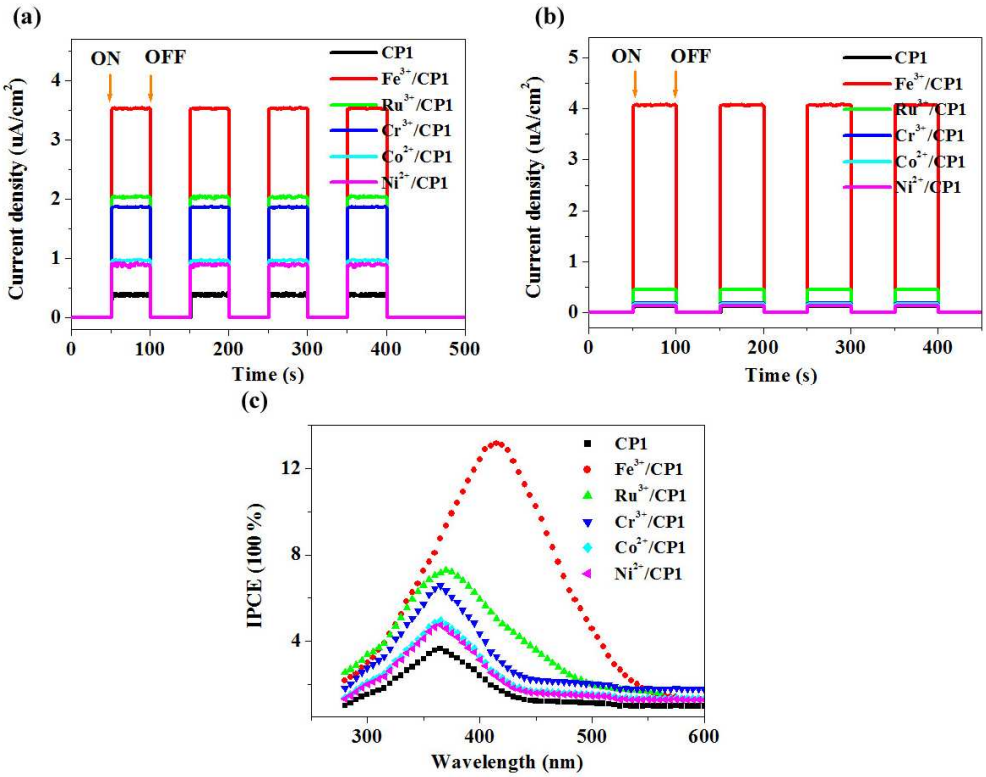

Figure 6

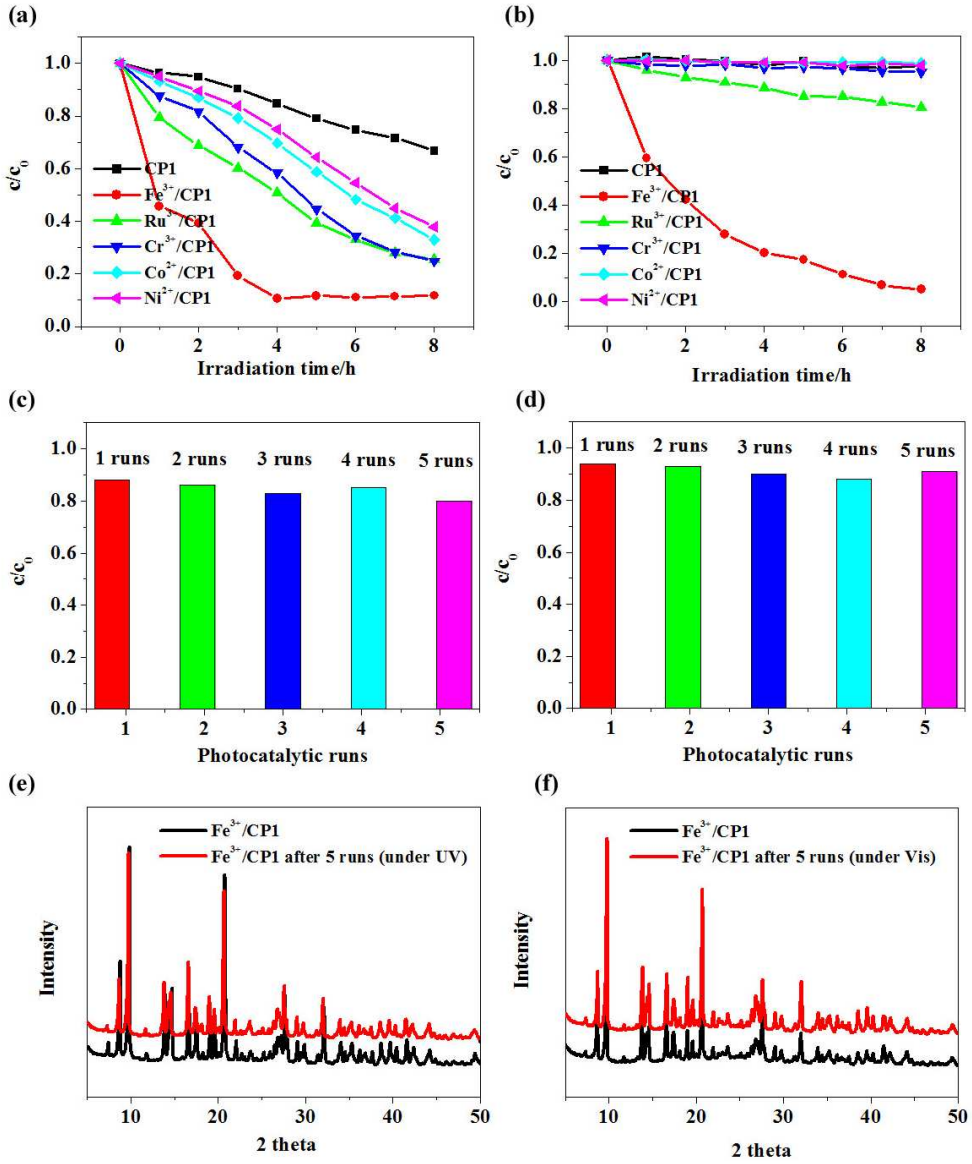

Figure 7